Applied Physics Letters ARTICLE pubs.aip.org/aip/apl

Evaluation of bias-dependent band structure changes in metal–oxide–semiconductor structures with varying doping concentrations using laboratory hard x-ray photoelectron spectroscopy

Cite as: Appl. Phys. Lett. **126**, 072103 (2025); doi: 10.1063/5.0245254
Submitted: 24 October 2024 · Accepted: 7 February 2025 ·
Published Online: 20 February 2025

Takuya Minowa,[1,a)] Koji Usuda,[2] Ryo Yokogawa,[1,2] and Atsushi Ogura[1,2]

AFFILIATIONS

[1]School of Science and Technology, Meiji University, 1-1-1, Higashimita, Tama-ku, Kawasaki, Kanagawa 214-8571, Japan
[2]Meiji Renewable Energy Laboratory, Meiji University, 1-1-1, Higashimita, Tama-ku, Kawasaki, Kanagawa 214-8571, Japan

[a)]**Present address**: Meiji University, 1-1-1, Higashimita, Tama-ku, Kawasaki, Kanagawa 214-8571, Japan. **Author to whom correspondence should be addressed:** tky.13579da.rt@gmail.com

ABSTRACT

Direct observation of the band structure variation of electrical devices, such as MOSFETs, during device operation is the most important for understanding MOSFET device operation. However, there are a few reports on the direct measurement of variation in the metal–oxide–semiconductor (MOS) interface band structure during operation, and further investigation is required. This paper focuses on elucidating the changes in the band structure at buried interfaces under applied bias using a nondestructive approach. We conducted measurements using bias-applied laboratory hard x-ray photoelectron spectroscopy (Lab. HAXPES) with liquid gallium (Ga) x-ray source on MOS structures, which are widely recognized as fundamental and commonly used devices. We utilize HAXPES with Ga x-ray, providing high-energy/intensity x-rays, to achieve sufficient detection depth and enable observation of the deeper regions of the silicon substrate buried under gold and silicon dioxide layers. As a result, this approach allowed us to observe bias-dependent peak shifts resulting from changes in the band structure in detail. We observe HAXPES peak shift caused by the different substrate concentrations. Additionally, we obtained detailed information on band bending by applying a wider range of bias compared to previous bias applied HAXPES.

Enhancing the performance of semiconductor devices is essential for realizing an Internet of Things society. In particular, interfaces are among the key factors determining device performance.[1,2] With the miniaturization and three-dimensional integration of semiconductor devices, interfaces have had increasingly significant impacts on the electrical properties of devices in recent years, particularly in advanced technologies such as gate-all-around transistors and memory devices optimized for artificial intelligence (AI) applications, where precise interface control is essential.[3–5] Therefore, understanding interfaces in detail is inevitable for improving the performance of advanced semiconductor devices. While there are many techniques for evaluating interfaces, methods for nondestructive and practical characterization of buried interfaces remain limited. If nondestructive and precise interface evaluation could be realized, understanding accurate interfaces identical to those in real devices would become feasible. Therefore, the immediate application of nondestructive interface structure analysis is essential.[6] Consequently, hard x-ray photoelectron spectroscopy (HAXPES) has gained much attention as a promising technique capable of nondestructively evaluating interfaces in multilayer film structures used in actual devices.

HAXPES is one of x-ray photoelectron spectroscopy (XPS) utilizing hard x-rays. The hard x-ray enhances the kinetic energy of photoelectrons. This leads to an increased inelastic mean free path for the photoelectrons, enabling a detection depth several times greater than that of conventional XPS.[7] Figure 1 shows the relationship between the excitation energy of incident x-rays and detection depth from a sample surface.[8] The signal intensity generally attenuates by approximately 95% at a distance three times the inelastic mean free path (IMFP), making this distance roughly equivalent to the detection depth. The figure confirms that HAXPES achieves more than twice the detection depth compared to conventional XPS. To obtain information about the silicon (Si) layer and/or the substrate beneath the electrode and

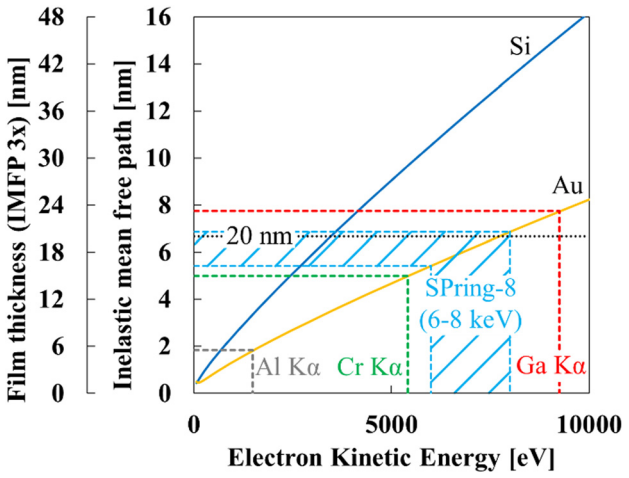

FIG. 1. Detection depth increases with a higher x-ray energy, as indicated by the black dotted line for a 20-nm-thick Au electrode. This demonstrates the enhanced capability of HAXPES for probing buried interfaces.[8]

oxide layer in a metal–oxide–semiconductor (MOS) structure, a detection depth of at least 40 nm from the surface is required. Based on IMFP estimations, it is clear that probing beneath the electrode [e.g., 20-nm gold (Au)] requires x-rays with a minimum energy of 8–10 keV. Therefore, gallium (Ga) Kα-based photoelectron spectroscopy is essential to achieve the objectives of this study. This advantage enables us to examine the characteristics of the entire MOS structure. However, as the energy of the x-rays increases, the photoionization cross section of light elements decreases significantly, resulting in reduced detection sensitivity.[9,10] Therefore, measurements are generally performed at synchrotron radiation facilities to enhance sensitivity, utilizing high-energy-resolution and high-brilliance x-ray sources.[11–14] However, the limited availability of beamlines at the facilities is a significant hurdle to conducting timely experiments. To solve these problems mentioned above, laboratory HAXPES (Lab. HAXPES) has been developed, and it uses a higher kinetic energy (K.E.) x-ray source and 5.4-keV chromium. However, requirements for measurements at a higher K.E. and necessary improvements in the hard x-ray intensity remain. Based on this background, laboratory-based high-energy x-ray sources with sufficient x-ray intensity and the K.E. have been developed, generating Ga x-ray around 9.25 keV by circulating liquid Ga alloy under a vacuum and irradiating it with an electron beam.[13] Using a monochromator with a high spectral resolution and intensity, a Si crystal with a 550-mm Rowland circle and keeping it at an elevated temperature enables the precise irradiation of narrow-bandwidth Ga x-ray onto samples.[15,16] These advantages are crucial for achieving deeper detection and greater immediacy, effectively addressing the limitations of the previous Lab. HAXPES.[17,18] Table I compares various photoelectron spectroscopy. It highlights that Lab. HAXPES, with its sufficient detection depth enabled by hard x-rays and real-time measurement capability, is a promising tool for industrial applications. Compared to the other nondestructive interface evaluation techniques, including spectroscopic ellipsometry and Raman spectroscopy, Lab. HAXPES demonstrates superior depth resolution. Detailed comparison results are provided in the supplementary material.

Conventional methods for evaluating MOS interface structures rely primarily on electrical characterization techniques such as capacitance–voltage (CV) measurement. However, there are limited examples of detailed analyses of electric potential distributions or band structure variations, such as the degree of band bending, under pseudo-operating conditions with applied bias. The use of Lab. HAXPES shows great promise for providing valuable insights that could enhance the performance of the next-generation scaled devices. For the purposes, preliminary studies on bias-applied photoelectron spectroscopy have been reported, although these studies were performed.[19–24] However, when a bias of, for example, 1 V is applied to a MOS structure, the potential is distributed across several layers, including the oxide layer. The potential reaching the underlying Si semiconductor layer is reduced to less than 1 V. Consequently, the band shift induced by the applied bias becomes smaller compared to the bandgap of Si, potentially limiting the ability to comprehensively analyze the band variations necessary to understand the operation of the MOS structure in the depth direction. To address this issue, it is necessary to increase the applied bias, for instance, up to 3 V. In addition, high excitation energy over 9 keV is required to achieve sufficient measurement depth to analyze the MOS structure under operating conditions. Therefore, HAXPES with Ga x-ray becomes essential for this purpose. Furthermore, to ensure immediacy and accessibility in the evaluation process, Lab. HAXPES has been introduced and investigated for its applicability to the analyses above. The results of this study are reported in the following sections.

The experimental procedure is outlined as follows. We prepared 20-nm Au/8-nm thermally oxidized SiO_2/*p*-type (001) Si substrate/200-nm aluminum (Al) as a standard MOS structure. Two types of Si substrates with different dopant concentrations were used, with resistivities of 5.70 and 0.49 Ω · cm. The details on the substrates used in

TABLE I. Comparison of Lab. XPS, Lab. HAXPES, and synchrotron radiation HAXPES at SPring-8 in Japan.

	Lab. XPS (Al Kα)	Lab. HAXPES (Ga Kα)	Synchrotron radiation HAXPES (at SPring-8)
Excitation x-ray energy	1.49 keV	9.25 keV	Mainly 6–8 keV
IMFP (Si)	3.37 nm	15.2 nm	10.5–13.4 nm
Resolution (Ag 3d5/2 Full width at half maximum)	∼0.5 eV	∼0.5 eV	∼0.2 eV
X-ray spot size	30 (V) × 30 (H) μm^2	30 (V) × 40 (H) μm^2	1 (V) × 30 (H) μm^2
Measurement time (Survey scan)	5 min	15 min	1 min
Turnaround time	Within a day	Within a day	A few month

TABLE II. Details of the MOS samples, including Si substrate resistivity and layer thickness.

Name	Type	Dopant	Thickness (μm)	Resistivity (Ω cm)	Impurity concentration (cm^{-3})
5.70 Ω cm sample	P	B	525 ± 25	5.70	2.43×10^{15}
0.49 Ω cm sample	P	B	625 ± 25	0.49	2.83×10^{16}

this study are shown in Table II. After forming thermal oxide films on the *p*-type Si substrates, Au was deposited as preventing the top electrode. Au is chemically stable, enabling low resistance and the formation of an interfacial layer. A layer 20 nm thick is thick enough to avoid Au cluster formation during the deposition. The oxide film on the back side was removed using dilute hydrofluoric acid, followed by the deposition of Al using resistance-heated vacuum evaporation. The thicknesses of each layer were confirmed using a cross-sectional scanning electron microscope and spectroscopic ellipsometry.

Bias-applied operando measurements of the MOS structure were performed using HAXPES equipped with an Excillum Ga source (Metal Jet D2+) and a Scienta Omicron analyzer (EW4000). Ga Kα ($h\nu = 9251.7$ eV) was used as the liquid Ga excitation x-ray source. HAXPES measurements were performed with a pass energy of 200 eV and an energy step of 50 meV. The measurement system is shown in Fig. 2(a), and the detection range is illustrated in Fig. 2(b). As shown in Fig. 2(b), the detection range of the excited photoelectrons included the Au layer (the top electrode), the SiO_2 layer, and part of the Si substrate. The surface electrode was grounded, and bias was applied at the rear Al electrode. Photoelectron spectra of Si 1s and Au 4f were acquired. The positions of the Si–Si and Si–O bonding peaks in the Si 1s spectra and the Au–Au bonding peaks in the Au 4f7/2 spectra were determined by peak fitting. The Voigt function and convolution of the Doniach–Sunjic function and the Gaussian function were used for the fitting function. The peak shifts were evaluated relative to the peak positions at a 0-V applied bias. The Au–Au bond peak comes from the surface electrode, the Si–O bond peak comes from the SiO_2 layer, and the Si–Si bond peak comes from the Si substrate.

Figure 3 shows the photoelectron spectra of Si 1s and Au 4f for various applied biases in the 5.70-$\Omega \cdot$cm sample. Focusing on Au 4f, the Au^0 (Au–Au) peak position remained constant before and after bias application, as it was grounded. In contrast, for Si 1s, distinct peak shifts in Si^{4+} (Si–O) and Si^0 (Si–Si) were observed with bias application. In other words, we observed the peak shifts of Au–Au, Si–O, and Si–Si corresponding to the direction of the bias applied to the MOS structure. From the results, it can be concluded that the behavior of each peak due to the bias applied to the samples was reasonable and that the application of potential to the samples worked correctly.

Figure 4 shows the applied bias dependence of the peak positions obtained by fitting the photoelectron spectra with the Voigt function and convolution of the Doniach–Sunjic function and the Gaussian function. The peak shifts were calculated from the difference between the peak positions at zero bias and each peak position when a potential was applied. It was confirmed that the Au–Au peak did not shift in response to changes in the applied bias. In comparison, the Si–Si peak shift on bias application is larger than that of the Si-O peak. These results suggest that potential changes in each layer of the MOS structure during bias application can be independently observed. Additionally, changes in peak shift amounts were observed around ± 1–1.5 V. Si substrates at different doping concentrations were further examined to confirm the mechanism of this change and the validity of the measurement. Comparing the 5.70 and 0.49-$\Omega \cdot$cm samples, differences in peak shifts of Si–O and Si–Si were observed due to the difference in the substrate concentration. It was also confirmed that the response rate to the applied bias in the peak shift depends on the substrate concentration. The reasons for this phenomenon will be discussed later.

Figure 5 shows the results of a simulation of the potential change based on one-dimensional Poisson's equation for the low bias application region (± 1 V), where the peak shifts linearly. Based on the

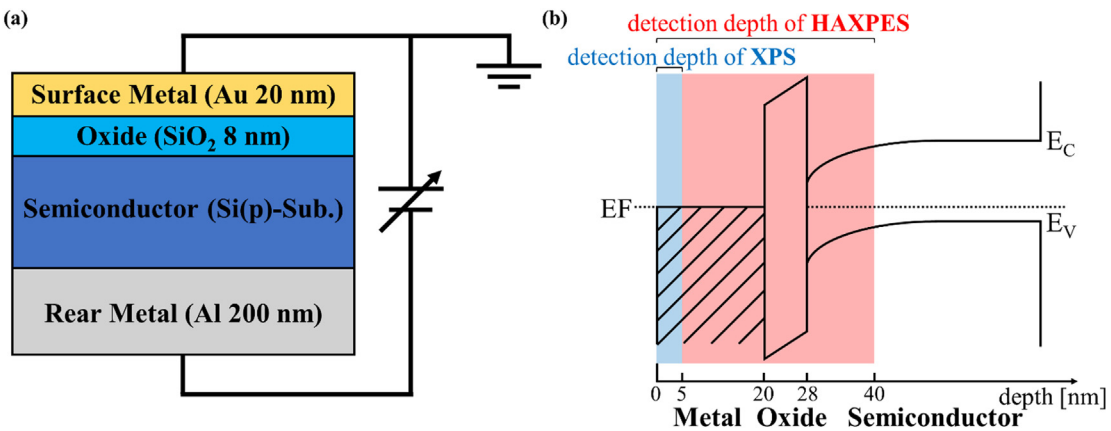

FIG. 2. (a) Relationship between detection depth and band structure under 0 V bias. (b) Schematic illustration of the MOS structure and the HAXPES measurement system, highlighting the detection range.

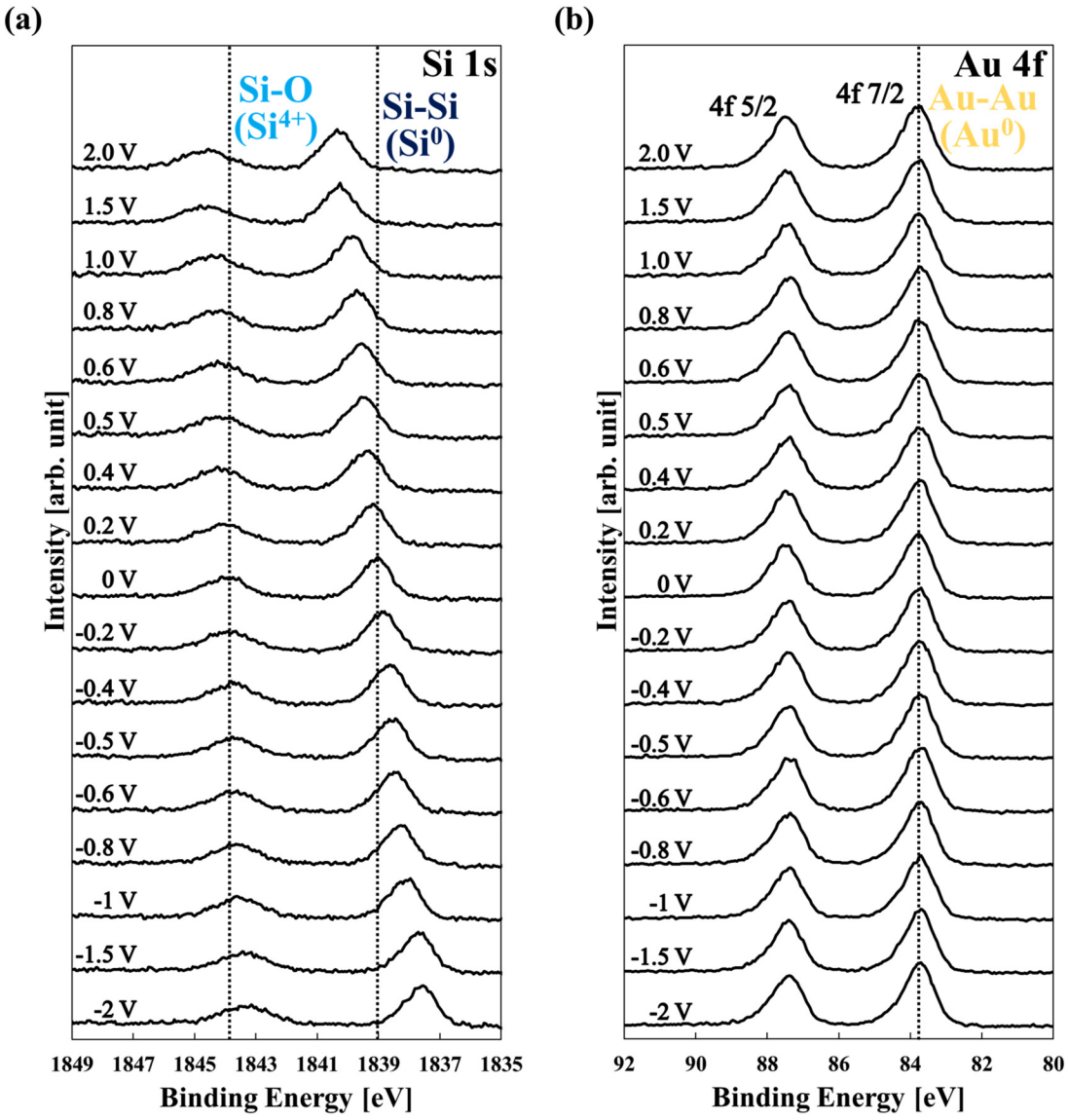

FIG. 3. (a) Si 1s and (b) Au 4f spectra for the 5.70-Ω·cm sample. Distinct peak shifts of Si 1s are observed, corresponding to changes in the applied bias.

Poisson equation used, the relationship between the potential and the carriers is shown as follows:[25,26]

$$\frac{d^2\Phi}{dy^2} = -\frac{q}{\varepsilon\varepsilon_0}\left[p_0\left\{\exp\left(-\frac{e\Phi}{kT}\right)-1\right\} - n_0\left\{\exp\left(\frac{e\Phi}{kT}\right)-1\right\}\right]. \quad (1)$$

Comparing the simulation results with the measurement results, we confirmed that the distribution of the potential and the relative amounts of the peak shift were consistent. The absence of fundamental discrepancies between the results and calculations suggests that the measurements were correct.

We discuss the bias dependence of the peak shifts, as demonstrated in the results. Refer to the supplementary material for the direction of band changes when applying bias with the surface electrode grounded. First, in Fig. 4(a), in the low bias application region (approximately ±0.5 V) of the 5.70-Ω · cm sample, where the effects of inversion and accumulation are minimal, the amount of peak shift for the Si–Si changed linearly with the applied bias. This indicates that the band bending changed linearly with the applied bias, resulting in the peak shift amount corresponding to the applied bias. On the other hand, when a negative bias was applied, the peak shift amount started to deviate from the linear change around −0.5 to −1.5 V, and an apparent decrease in the shift amount was observed. Considering the concentration of the Si substrate, this region is thought to correspond to the weak inversion region. We consider that the change in band bending is suppressed as acceptor ions and electrons gradually

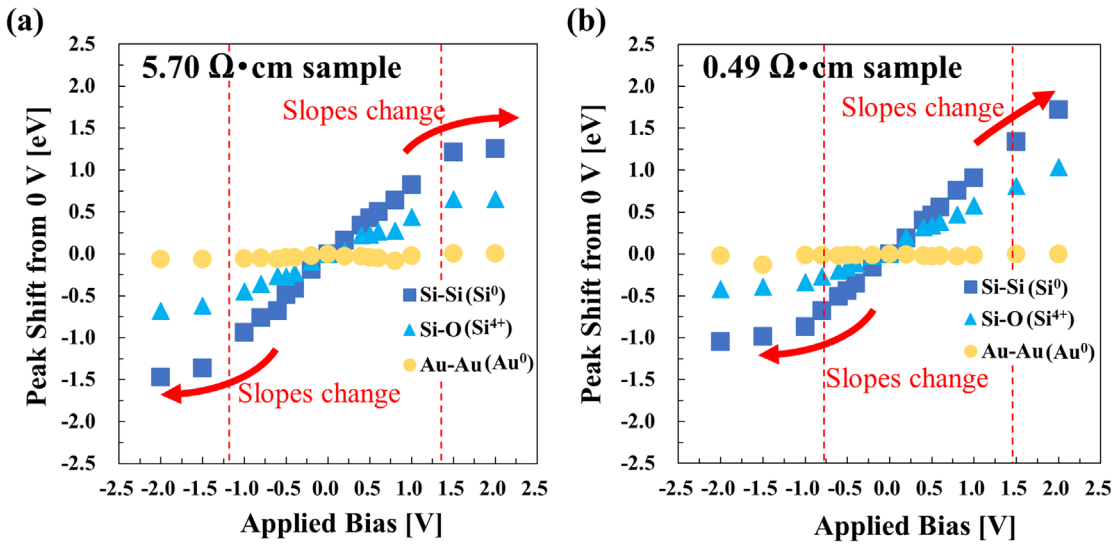

FIG. 4. Peak shifts relative to zero bias for (a) the 5.70-Ω·cm and (b) the 0.49-Ω·cm samples. The dotted lines mark the bias points where the rate of peak shift begins to deviate from linearity.

neutralize during the transition toward strong inversion, so the corresponding changes in the band structure were observed. A distinct change in the peak shift amount was observed under conditions where the bias was further applied beyond −1.5 V. These results show that the variation width of the peak shift from the linear change significantly decreased. This also suggests a strong inversion state in the Si layer. Band bending is a phenomenon where the band bends due to charges accumulated at the SiO_2/Au interface. In the strong inversion region, inversion electrons emerge, suppressing the accumulation of holes at the SiO_2/Au interface. As a result, band changes do not occur in the strong inversion region, and the band becomes fixed. Therefore, it is thought that only the resistances of the oxide film, the depletion layer, and the intrinsic substrate contribute to the change in the peak position.

Next, when a positive bias was applied, we observed that around 0.5–1.5 V, similar to the negative bias, the peak shift amount started to deviate from the linear behavior with respect to the applied bias. This situation reflects the Si layer transitioning into an accumulation state. As the potential further increased beyond 1.5 V, a distinct change in the peak shift amount was also observed, like in the case of the application of negative bias. This is likely due to the metallic behavior of the accumulation layer, which suppresses or fixes band changes during bias application. As a result, a potential gradient forms on the substrate side outside the detection range, causing the resistances of the oxide film and the intrinsic substrate to dominate the peak shift more directly.

The factors influencing the change in the peak shift amount of Si–Si are as follows. In the region where the peak shift amount changes, it is primarily due to the band bending of the Si layer. In the weak inversion region, the influence of band bending gradually weakens, and in the strong inversion region, the resistances of the oxide film and the intrinsic substrate become dominant. On the other hand, in the accumulation region, the resistances of the oxide film and the intrinsic substrate are the controlling factors.

Figure 4(b) illustrates that, for the 0.49-Ω · cm sample, in the low bias application region (−0.25 to 0.75 V), a linear correlation existed between the applied bias and the Si–Si peak shift amount, analogous to the observations made for the 5.70-Ω · cm sample. It is postulated that this shift is due to the band bending at 0 V being larger due to the lower resistance of Si, which causes the entire region to shift toward the positive bias side. When negative bias was applied, the peak shift amount began to deviate from linearity between −0.25 and −1.0 V. This is attributed to band changes observed in the weak inversion region. Furthermore, in the region where a bias exceeding −1.0 V was applied, peak shift amount changes comparable to those observed at −1.5 V for the 5.70-Ω · cm sample were noted. For the low-resistance 0.49-Ω · cm sample, the higher impurity concentration resulted in a smaller maximum depletion layer width, causing the depletion layer to reach its maximum at a lower negative bias. This difference is attributed to the variation in the applied bias values that cause peak shift changes between the two different substrates, namely, −1.0 and −1.5 V. Furthermore, when positive bias was applied, analogous to the 5.70-Ω · cm sample, alterations in band bending and peak displacement due to band fixation in the accumulation region were discerned. However, for the low-resistance 0.49-Ω · cm sample, the higher impurity concentration resulted in a greater carrier density, thereby causing the substrate outside the depletion layer to exhibit more metallic behavior. Consequently, more linear peak shift changes were observed compared to the 5.70-Ω · cm sample. This indicates not only the observation of band changes due to differences in the impurity concentration but also that the results are consistent with qualitative explanations. On the other hand, discrepancies between the simulation results and experimental data under negative bias application have been observed. These differences are presumed to arise, at least in part, from the uncertainty of Au work function. Specifically, the work function of Au varies significantly depending on the literature source,[27,28] and the value adopted in this study may not match that of the actual sample, leading to the observed

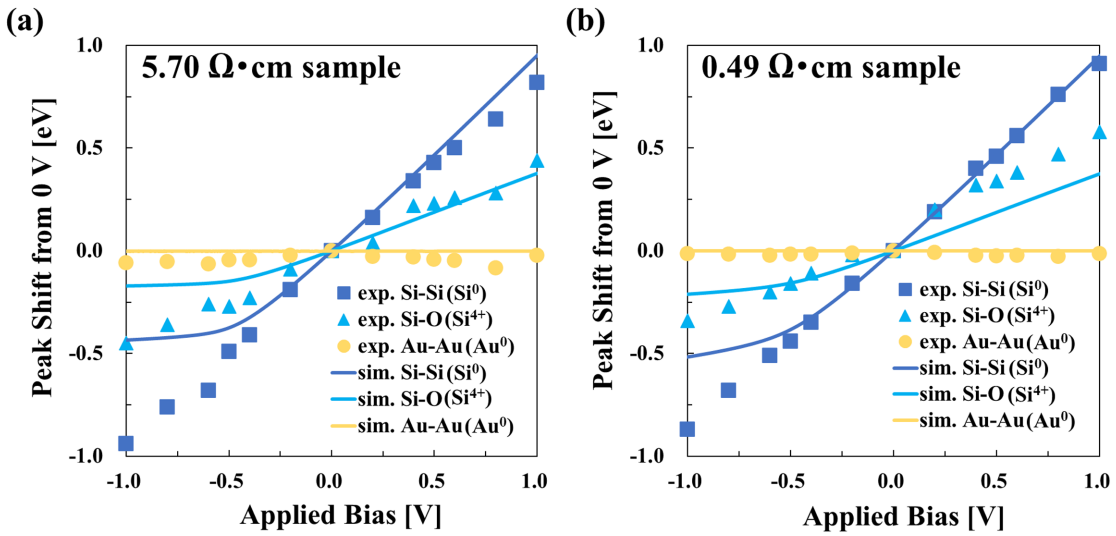

FIG. 5. Simulation results based on Poisson's equation for (a) 5.70-Ω · cm and (b) 0.49-Ω · cm samples. Linear peak shifts are observed in the low-bias region, consistent with experimental results.

discrepancies. Determining the precise work function of Au remains a subject for future investigation.

In summary, using Lab. HAXPES with Ga x-ray, we achieved more accurate band structure analysis by enabling deeper layer observation and extending evaluations to phenomena in the accumulation and inversion layers under high applied bias conditions. By utilizing this method, we evaluated fundamental MOS structures using operando techniques and found that band structure changes depended on the substrate resistance. Consequently, in the 5.70-Ω · cm sample, apparent changes in the peak shift amount were observed, likely caused by band bending due to weak inversion, strong inversion, and accumulation layer formation. Additionally, we identified band bending behaviors in the 0.49-Ω · cm sample with a higher substrate concentration, including narrower depletion layers and more linear peak shifts in the accumulation region, which were confirmed thanks to the wider voltage rage measurement of ±3 V rather than ±1 V and consistent with qualitative predictions. Therefore, bias-applied operando measurements using Lab. HAXPES with Ga x-ray source are expected to be a highly practical and nondestructive method for evaluating buried interfaces in multilayer films of actual devices.

See the supplementary material for the details on the experimental setup, including the Lab. HAXPES system schematics, grounding configurations, and measurement conditions; extended data, including photoelectron spectra under various biases; fitting parameters for Si 1s and Au 4f peaks; and comparisons with other analytical techniques.

We are grateful for the useful comments we received from the KIOXIA Corporation at the beginning of the equipment launch period. Their support was instrumental in the development of this study.

AUTHOR DECLARATIONS

Conflict of Interest

The authors have no conflicts to disclose.

Author Contributions

Takuya Minowa: Conceptualization (equal); Data curation (equal); Formal analysis (equal); Investigation (equal); Methodology (equal); Resources (equal); Software (lead); Validation (equal); Writing – original draft (equal); Writing – review & editing (equal). **Koji Usuda:** Conceptualization (equal); Investigation (equal); Methodology (equal); Resources (equal); Writing – original draft (equal); Writing – review & editing (equal). **Ryo Yokogawa:** Conceptualization (equal); Funding acquisition (lead); Investigation (equal); Methodology (equal); Project administration (equal); Resources (equal); Supervision (lead); Writing – review & editing (equal). **Atsushi Ogura:** Conceptualization (equal); Funding acquisition (lead); Investigation (equal); Methodology (equal); Project administration (equal); Resources (equal); Supervision (lead); Writing – original draft (equal); Writing – review & editing (equal).

DATA AVAILABILITY

The data that support the findings of this study are available from the corresponding author upon reasonable request.

REFERENCES

[1]Y. Gao, Mater. Sci. Eng., R **68**, 39–87 (2010).
[2]R. A. Mckee, F. J. Walker, and M. F. Chisholm, Science **293**, 468–471 (2001).
[3]A. Beyer, A. Stegmüller, J. O. Oelerich, K. Jandieri, K. Werner, G. Mette, W. Stolz, S. D. Baranovskii, R. Tonner, and K. Volz, Chem. Mater. **28**, 3265–3275 (2016).
[4]V. Mirsa, G. Lucovslky, and G. Parsons, MRS Bull. **27**, 212–216 (2002).
[5]E. H. Poindexter, Semicond. Sci. Technol. **4**, 961–969 (1989).
[6]M. J. Deen and F. Pascal, J. Mater. Sci.-Mater. Electron **17**, 549–575 (2006).
[7]S. Tanuma, C. J. Powell, and D. R. Penn, Surf. Interface Anal. **43**, 689–713 (2011).
[8]H. Shinotsuka, S. Tanuma, C. J. Powell, and D. R. Penn, Surf. Interface Anal **47**, 871–888 (2015).
[9]J. J. Yeh and I. Lindau, At. Data Nucl. Data Tables **32**, 1–155 (1985).
[10]B. F. Spencer, S. Maniyarasu, B. P. Reed, D. J. H. Cant, R. Ahumada-Lazo, A. G. Thomas, C. A. Muryn, M. Maschek, S. K. Eriksson, T. Wiell, T.-L. Lee, S. Tougaard, A. G. Shard, and W. R. Flavell, Appl. Surf. Sci. **541**, 148635 (2021).

[11]L. Kövér, J. Electron Spectrosc. Related Phenom. **178-179**, 241–257 (2010).
[12]T. Watanabe, K. Tada, S. Yasuno, H. Oji, N. Yoshimoto, and I. Hirosawa, Jpn. J. Appl. Phys., Part 1 **55**, 03DD12 (2016).
[13]D. H. Larsson, P. A. C. Takman, U. Lundström, A. Burvall, and H. M. Hertz, Rev. Sci. Instrum. **82**, 123701 (2011).
[14]M. Gorgoi, S. Svensson, F. Schäfers, W. Braun, and W. Eberhardt, Eur. Phys. J. Spec. Top. **169**, 221–225 (2009).
[15]A. Regoutz, M. Mascheck, T. Wiell, S. K. Eriksson, C. Liljenberg, K. Tetzner, B. A. D. Williamson, D. O. Scanlon, and P. Palmgren, Rev. Sci. Instrum. **89**, 073105 (2018).
[16]B. F. Spencer, S. A. Church, P. Thompson, D. J. H. Cant, S. Maniyarasu, A. Theodosiou, A. N. Jones, M. J. Kappers, D. J. Binks, R. A. Oliver, J. Higgins, A. G. Thomas, T. Thomson, A. G. Shard, and W. R. Flavell, Faraday Discuss. **236**, 311–337 (2022).
[17]J. F. Watts and J. E. Castle, Surf. Interface Anal. **56**, 408–424 (2024).
[18]D. Zheng, C. N. Young, and W. F. Stickle, Surf. Sci. Spectra **30**, 024004 (2023).
[19]Y. Yamashita, H. Yoshikawa, T. Chikyow, and K. Kobayashi, J. Appl. Phys. **113**, 163707 (2013).
[20]Y. Yamashita, H. Yoshikawa, T. Chikyo, and K. Kobayashi, J. Appl. Phys. **115**, 043721 (2014).
[21]Y. Yamashita, K. Ohmori, S. Ueda, H. Yoshikawa, T. Chikyow, and K. Kobayashi, e-J. Surf. Sci. Nanotechnol. **8**, 81–83 (2010).
[22]L. A. Walsh, G. Hughes, J. Lin, K. Hurley, T. P. O'Regan, E. Cockayne, and J. C. Woicik, Phys. Rev. B **88**, 045322 (2013).
[23]K. Kobayashi, M. Kobata, and H. Iwai, J. Electron Spectrosc. Relat. Phenom **190**, 210–221 (2013).
[24]O. Renault, P.-M. Deleuze, J. Courtin, T. R. Bure, N. Gauthier, E. Nolot, C. Robert-Goumet, N. Pauly, E. Martinez, and K. Artyushkova, Faraday Discuss. **236**, 288–310 (2022).
[25]S. Toyoda and M. Oshima, J. Appl. Phys. **120**, 085306 (2016).
[26]R. Z. Wang, B. Wang, H. Wang, H. Zhou, A. P. Huang, M. K. Zhu, H. Yan, and X. H. Yan, Appl. Phys. Lett. **81**, 2782–2784 (2002).
[27]N. Mahmoodi, A. I. Rushdi, J. Bowen, A. Sabouri, C. J. Anthony, P. M. Mendes, and J. A. Preece, J. Vac. Sci. Technol., A **35**, 041514 (2017).
[28]F. Ruffino and M. G. Grimaldi, Coatings **8**, 121 (2018).